ON THE CRYSTALLOGRAPHY OF PERITECTIC AUSTENITE AND THE ROLE OF PRIMARY FERRITE IN HIGH MANGANESE AND ALUMINUM STEELS

M. McGrath and D. Van Aken
Missouri University of Science and Technology, Rolla, MO, USA

Abstract

Two high manganese and aluminum steels with duplex microstructures of δ-ferrite and austenite, having different weight fractions of primary δ-ferrite (0.35 vs. 0.66), were used to study the crystallography of austenite formed during the peritectic reaction. Electron backscattered diffraction (EBSD) was used to characterize the crystallographic growth directions and orientation relationships between the two phases. For a primary δ-ferrite weight fraction of 0.66, the peritectic austenite product was seven times more likely to have the Kurdjumov-Sachs (K-S) orientation relationship. In contrast, a lower weight fraction of δ-ferrite produced a peritectic reaction where both δ-ferrite and the peritectic austenite product grew with the same <100> or <110> parallel to the heat flux. The K-S orientation was observed for only 5% of the peritectic interfaces. Manganese and aluminum solute profiles across the peritectic interface were used to show that the mechanism of the peritectic reaction remains the same for each alloy. Thermal analysis was used to compare the two alloys at the dendrite coherency point and the alloy with the smaller fraction of primary δ-ferrite had a greater solid fraction (0.4 versus 0.34) at the dendrite coherency point.

Keywords: *peritectic solidification, retained austenite, δ-ferrite, Fe-Mn-Al-C, EBSD, crystallography, cast steel, dendrite coherency point*

Introduction

Extensive deformation processing makes the crystallography of the peritectic reaction irrelevant for most wrought steel products. This is not true for castings or for ultra-thin cast strip products where post solidification deformation is non-existent or minimal. Thus, the crystallographic texture developed for castings and ultra-thin cast strip is of some importance with regard to properties and performance. For example, duplex and austenitic cast stainless steels will maintain the cast crystallographic texture, since grain refinement resulting from the austenite to α-ferrite (A_3) transformation is not feasible by normalization heat treatments. Cast textures may play a role in the stress corrosion cracking and fatigue performance of duplex stainless steels where δ-ferrite and austenite are present in equal volumes. Stress corrosion cracking of ferrite is along {010} in chloride solutions[1] and the cast crystallography of δ-ferrite in the columnar zone is expected to play an important role. Fatigue initiation in duplex stainless steels is sensitive to the crystallography of the ferrite and austenite interface. In duplex stainless steels fatigue crack initiation is associated with grain boundary or interphase cracking.[2] In wrought duplex stainless steels, grain cracking between two ferrite grains initiates the short-crack fatigue behavior.[2] It should be noted that the majority of ferrite and austenite interfaces are parallel to the rolling direction in the wrought product. In cast duplex stainless steels fatigue crack initiation will begin by interphase cracking. The crystallography of the interphase boundary plays an important role in determining if the interface boundary cracks or does not crack under cyclic loading.[3] If the ferrite and austenite grains exhibit the Kurdjumov-Sachs (K-S) orientation relationship, the slip occurring in the austenite during cyclic loading is more easily accommodated by the ferrite and interphase cracking does not occur. In contrast, interface cracking initiates the fatigue crack when the K-S relationship is absent.[3] In low cycle fatigue, where crack propagation controls the cyclic life, the K-S orientation relationship promotes crack propagation through the interphase boundary and increases the rate of fatigue crack propagation. In contrast, the fatigue crack is deflected by interphase boundaries where the K-S orientation relationship is absent. It would therefore be important to fully understand the role of the peritectic reaction in the determination of interphase crystallography.

For steel solidification, the primary δ-ferrite is expected to grow with <100> parallel to the heat flux.[4-7] The peritectic reaction has been described as austenite nucleating on the liquid/δ-ferrite interface[8,9] with subsequent growth along the δ-ferrite/liquid interface as alloy is rejected into the liquid by the two solids.[8,10-15] Several authors have indicated that the reaction proceeds at the triple point junction formed by liquid, δ-ferrite, and austenite.[8,14-16] Once the δ-ferrite is encapsulated by austenite and the δ-ferrite is no longer in contact with liquid, the austenite growth or peritectic transformation occurs by long range diffusion.[9] This peritectic transformation of δ-ferrite to austenite will be small relative to the peritectic reaction if the diffusion rates are small.[17] Shibata et al.[14] has reported that the rate of the peritectic reaction in undercooled liquid steel was not controlled by carbon diffusivity in liquid as previously suggested by Bosze and Trivedi.[16] Shibata et al.[14] concluded that the majority of the austenite formed by a massive transformation or direct solidification of austenite from the liquid after the peritectic reaction formed a thin layer of austenite on the ferrite. Dhindaw et al.[15] supported those conclusions by reporting no evidence of alloy partitioning in a steel of composition Fe-0.22C-1.3Cr-2.6Ni.

In 1965, Hu[18] showed that the K-S orientation relationship applied to the solid-state (A_4) transformation of δ-ferrite to austenite in a zone melted iron bar and Hu was able to predict the crystallography of the α-ferrite, which was observed based upon applying the K-S relationship to both the A_4 and A_3 solid state transformations. If the austenite forms by primary solidification, the growth direction is reported to be either <110>[4] or <100>,[4-7] which would preclude the K-S relationship when the δ-ferrite also has a <100> growth. This fact has been discussed by Inoue et al.[19] where the imposed temperature gradient favors specific growth directions for

Table 1. Crystallographic Relationships Observed between δ-Ferrite and Austenite

Alloy System	Solidification Process	Observation	Reference
Fe-Cr-Ni containing 17 to 80% residual δ-ferrite	Electrode and SMA Weld with Filler	<100> direction in the ferrite was parallel to the heat extraction while the <100> and <110> directions of the austenite were parallel to the heat extraction	4
Fe-Cr-Ni containing between 4 to 18% residual δ-ferrite	Autogeneous GTA and SMA Welds	K-S type orientation relationship existed between lathy δ-ferrite and austenite (faceted interfaces) while austenite did not establish an orientation relationship with the vermicular ferrite	21
Fe-Cr-Ni containing 28.5% residual δ-ferrite	Casting	K-S orientation relationship existed between faceted δ-ferrite/austenite interfaces	21
Fe-Cr-Ni	Laser Resolidification	When ferrite was the primary phase austenite growth was in the same orientation as the ferrite	23
Fe-Cr-Ni containing 5 to 13% residual δ-ferrite	Autogeneous GTA Weld	Austenite establishes a K-S orientation relationship, parallelism between <100> crystallographic growth direction, or a parallel relationship between close-packed planes with ferrite. This relationship affected the ferrite morphology.	5
304L	LENS-Fabricated	New orientation relationship observed (see Table 2 for Headley-Brooks) while the frequency of observation was quite low	24
309S	Autogeneous GTA weld		
Fe-Cr-Ni	Autogeneous GTA weld		
316L containing 3.9 to 5.9% residual δ-ferrite	Bottom Poured Cast Ingots	Headley-Brooks orientation relationship observed and faceted interfaces suggested an orientation relationship existed between the ferrite and austenite	25
310S	Laser Spot Welds	Austenite showed epitaxial growth from a grain in heat affected zone (HAZ) with the <100> directions aligned of the two grains.	6
304	GTA Welds, Laser Spot Welds	Various ferrite growth directions were observed through the fusion zone (FZ). The austenite crystallographic growth direction was not parallel with the ferrite.	
Fe-Cr-Ni	Autogeneous GTA Weld	Austenite nucleated without contact of δ-ferrite would not be restricted crystallographically by ferrite and thus the two phases grow independently.	26
YUS701 (Incoloy)	Manual Arc Welding with no δ-ferrite Formation	Austenite grains grew epitaxially from base metal but <100> growth direction was more favorable direction	7

the δ-ferrite and austenite rather than a specific crystallographic orientation relationship between the two solids.

Nucleation of the peritectic solid product can also occur without contact with the primary phase as observed by Fredriksson et al.[20] in directionally solidified Al-Mn alloys. For the Al-Mn peritectic the liquid separates the two solids and solute diffuses through the liquid for growth of the peritectic solid product. However, austenite nucleation and growth without contact with δ-ferrite is rarely described as a mechanism in steel literature.[15] Often undercooling below the peritectic temperature is a requirement for direct nucleation of austenite.[17] Most of the crystallographic studies for the peritectic reaction in steel have been performed on stainless steel welds and very few studies on castings as shown in Table 1. Alloy composition and cooling rates have been shown to produce different δ-ferrite morphologies.[5,11,19,26-29] Brooks et al.[11] described skeletal or vermicular ferrite as being located at the core of the solidified dendrite. Elmer et al.[27,28] also noted that vermicular ferrite has defined secondary arms separated by austenite. Lathy ferrite having a plate-like appearance with faceted interfaces was also described by Brooks et al.[11] as being confined to the core of the dendrite. The ferrite observed by Brown et al.[22] was described as engulfing the austenite where the δ-ferrite was present in quantities greater than 25%. Brown et al.[22] also reported faceting of the δ-ferrite and austenite interfaces. Several studies[21,22,25] reported that these faceted interfaces have the K-S orientation relationship. Table 2 shows the orientation relationships reported previously for the peritectic reaction in steels.[24,30] Headley and Brooks (H-B)[24] reported a new orientation relationship between ferrite and peritectic austenite observed in welds as having parallel <110> with closest packed planes being parallel (Table 2).

Little has been done to compare the crystallography observed in weld studies to that observed in cast metals. In weld studies the initial solidification will be dependent upon the crystallography of the grains in the heat affected zone. Castings will exhibit a chill zone where many new solid nuclei form on the mold wall and a few are selected with favorable orientation to grow into the liquid, which forms the columnar zone. The same may be true for the peritectic austenite where rapid peritectic growth of a favorably oriented austenite grain dominates (Figure 1). An equiaxed zone may also develop towards the center of the casting where primary δ-ferrite is randomly orientated.[31] However, no conclusive arguments have been proposed for the dependence of the peritectic austenite crystallography on the weight fraction of δ-ferrite formed during solidification. The purpose of this paper was to determine if the amount of primary δ-ferrite affected the crystallography and growth mechanism of austenite formed during the peritectic reaction in alloys cast in sand molds.

Recent investigations of high aluminum and manganese steels have produced duplex steels with varying amounts of δ-ferrite in the cast microstructure. The aluminum content was varied between 3 and 5 weight % in an effort to lower the steel density and meet property goals set for third generation advanced high strength steels (AHSS), which are targeted for automotive applications.[32-35] The solidified microstructures of these alloys often consist of δ-ferrite remnants in the dendrite cores along with retained austenite and secondary ferrite in the interdendritic regions. These new steels provide an opportunity to further investigate the peritectic reaction and results should be applicable to cast duplex stainless steels.

Procedure

Two Fe-Mn-Al-Si-C alloy compositions were chosen to study the peritectic reaction with respect to the amount of primary δ-ferrite formed. Chemical compositions for alloys P1 and P2 are provided in Table 3. These alloys were produced in a 45 kg (99 lbs) coreless induction furnace under an argon protective atmosphere using high purity iron,

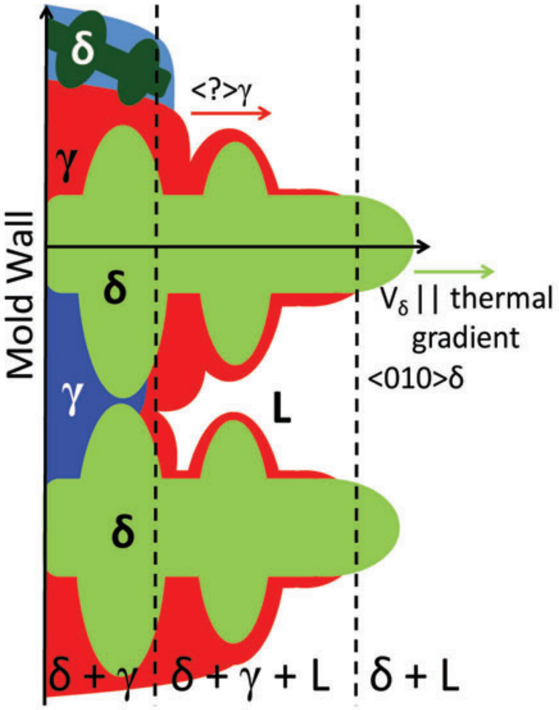

Figure 1. Schematic showing growth of primary ferrite (δ) with respect to austenite (γ). Growth directions are dependent on thermal and composition gradients.

Table 2. Known Orientation Relationships between Ferrite (BCC) and Austenite (FCC)

Name	Orientation Relationship
Kurdjumov-Sachs (K- S)[30]	$(111)_{fcc}//(110)_{bcc}$, $[0\bar{1}1]_{fcc}//[\bar{1}11]_{bcc}$
Headley-Brooks (H-B)[24]	$(111)_{fcc}//(110)_{bcc}$, $[\bar{1}10]_{fcc}//[\bar{1}10]_{bcc}$

electrolytic manganese, aluminum, ferrosilicon and carbon. Horizontal bar molds were prepared using phenolic no-bake olivine sand designed to produce a 20 cm long x 3 cm diameter (7.9 in. x 1.2 in.) bar as shown in Figure 2. A large center riser with 15 cm (5.9 in.) of head height over the horizontal bar was used for the studies reported in this paper. Cooling curves were obtained by pouring the melt into a thermal analysis cup with an S-type thermocouple located in the center of the cup. Alloy P2 was poured into an insulated cup whereas alloy P1 was poured using a configuration as described by Lekakh and Richards.[36] Temperature and time were recorded with a digital acquisition system. The thermal analysis data was used to calculate the fraction of the solid using a Newtonian heat balance model based on a zero line calculation proposed by Djurdjevic et al.[37]

Liquidus, peritectic, and solidus temperatures were calculated using Factsage[38] (hereafter known as Software A) version 6.2 to compare with measured values obtained from the thermal analyses. Software A[38] was also used to predict the weight fractions of phases as function of temperature and composition. The "FStel" database was used for "Fe-BCC," "Fe-FCC," and "Fe-Liquid" phases.

Specimens of dimension 2 mm x 12 mm x 10 mm (0.08 in. x 0.5 in. x 0.4 in.) for electron backscattered diffraction (EBSD) analysis were sectioned 3 cm (1.2 in.) from the bottom of the riser and 9 cm (3.5 in.) from the ends of the casting as shown in Figure 2. Specimens were mechanically polished using standard metallographic techniques with the final polishing step using vibratory polishing and 0.03µm colloidal silica. The EBSD analysis was performed on an FEI Helios NanoLab dual focused ion beam scanning electron microscope with an HKL EBSD system using a Flamenco-Acquisition software package. The accelerating voltage was at 15 kV with a probe current of 2.7 nA. An indexing rate of at least 85% was achieved for the analyzed specimens.

Results

Thermodynamic Calculations of Phase Equilibria

Vertical section phase diagrams were calculated using Software A[38] for a nominal Fe-14.2Mn-4.5Al-1.9Si-0.16C-0.0285N alloy with manganese and aluminum as composition variables (Figure 3). The two alloys are designated as P1 and P2 in the phase diagrams. The amount of primary δ-ferrite was dependent principally on the aluminum content as compared to the other alloying elements. Thermodynamic calculations for the amount of primary δ-ferrite formed for each specific alloy were determined using a Scheil algorithm and are shown in Figure 4.

The maximum primary δ-ferrite formed in weight fraction was 0.35 at 1400°C (2552°F) and 0.66 at 1350°C (2462°F) in alloys P1 and P2, respectively. The initial austenite in P1 and P2 was predicted to form through a peritectic reaction, where the δ-ferrite reacted with the liquid to form austenite and Figure 4 shows a decrease in δ-ferrite as austenite forms. Thermodynamic analysis of solute segregation during solidification (Scheil algorithm) identified the first δ-ferrite to form as being rich in aluminum and lean in manganese while the last liquid to solidify to austenite is rich in manganese and lean in aluminum for both alloys.

Thermal Analyses with Different Amounts of Primary Ferrite

Thermal analyses for both alloys are shown in Figure 5. The liquidus and solidus temperatures were determined based on the first derivative of temperature with respect to time. The measured liquidus temperatures were greater than the equilibrium predictions by 12 to 17°C (21.6 to 30.6°F). The solidus temperature for P1 was 7°C (12.6°F)

Table 3. Alloy Compositions in Weight Percent

	Mn	Al	Si	C	N	P	Fe
P1	13.56	3.44	2.10	0.20	0.013	0.012	bal.
P2	14.77	5.58	1.79	0.12	0.044	0.022	bal.

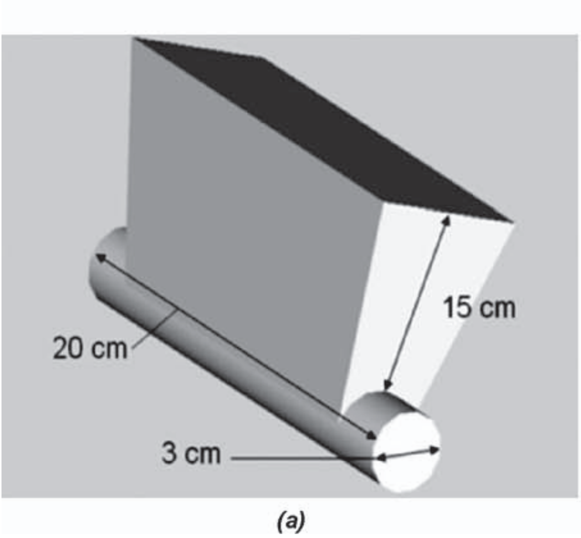

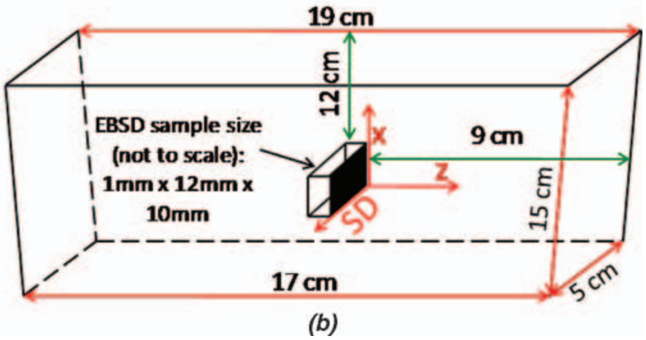

Figure 2. (a) CAD drawing of casting with dimensions given in cm. (b) Schematic showing the location of EBSD sample relative to the riser. SD symbolizes solidification direction.

greater than the Scheil prediction (1300°C [2372°F] as shown in Figure 4a). The experimentally measured solidus temperature of P2 was 151°C (271.8°F) greater than the temperature predicted by Scheil model (1245°C [2273°F] as shown in Figure 4b).

The fraction of solid is shown in Figure 6 as a function of temperature. Alloy P1 shows multiple changes in the rate of solid formation with undercooling below the liquidus temperature, which correspond to thermal arrest temperatures. A larger amount of undercooling (approximately 145°C [261°F]) was observed in P1 in order to solidify the remainder of the melt after the first thermal arrest. A comparison of the calculated and measured temperatures for the liquidus and solidus is presented in Table 4. This table also contains the calculated and measured weight fractions (W_f) of δ-ferrite at the peritectic and solidus temperatures. The fraction of δ-ferrite at the peritectic temperature was determined from Figure 6 at the first thermal arrest upon undercooling. The volume fraction (converted to weight fraction in Table 4) of δ-ferrite at the solidus temperature was measured by quantitative metallography using as-solidified microstructures from the columnar zone.

Microstructural Analysis of Sand Castings with Different Amounts of Primary Ferrite

Representative as-solidified microstructures from close to the mold wall and from the center of the riser are shown in Figure 7 for P1 and P2, where the mold wall was located at the top of each image. Structures near the mold wall were dendritic and the dendrites grew parallel to the expected heat

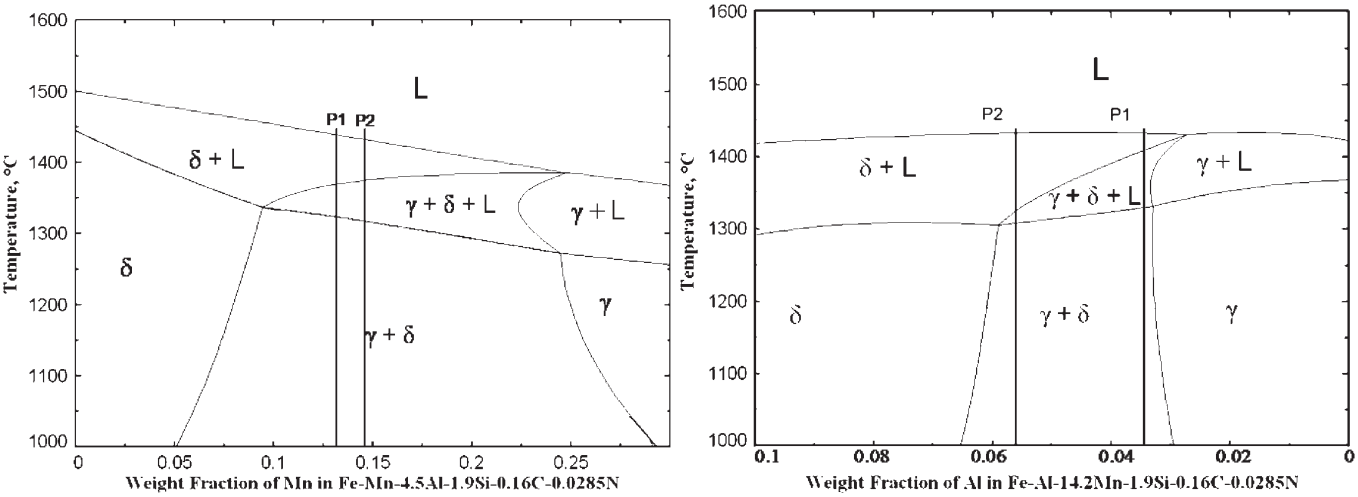

(a) *(b)*

Figure 3. Phase equilibrium diagrams constructed using Software A[38] with varying (a) manganese and (b) aluminum concentrations at various concentrations for (a) Fe-Mn-4.5Al-1.9Si-0.16C-0.0285N and (b) Fe-Al-14.2Mn-1.9Si-0.16C-0.0285N. The base compositions in (a) and (b) represent an average for both P1 and P2. Symbols (L = liquid, δ= ferrite and γ = austenite) were used to label phase regions.

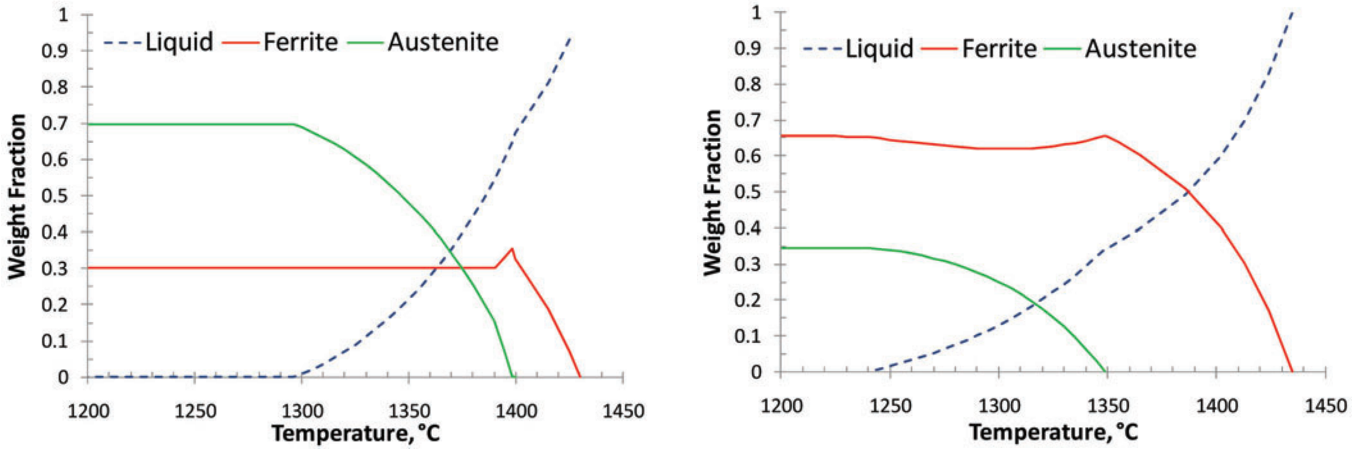

(a) *(b)*

Figure 4. Software A[38] Scheil predictions for solidification of alloy (a) P1 and (b) P2. Primary ferrite is predicted to form first at 1430°C (2606°F) and 1435°C (2615°F) in alloys P1 and P2, respectively. Austenite begins formation at 1400°C (2552°F) and 1350°C (2462°F) in alloys P1 and P2, respectively.

flux to produce a columnar zone. The primary δ-ferrite and austenite interfaces at the center of the castings appear to be more faceted and the dendrites were randomly oriented as expected for the equiaxed zone. A skeletal or vermicular δ-ferrite morphology was formed in both the columnar and equiaxed zones for P1. An engulfing δ-ferrite morphology was observed for P2 in the columnar zone and a lath- or plate-like structure was observed in the equiaxed zone. Secondary α-ferrite was present in P1 and was located near the δ-ferrite. The weight fraction of austenite measured in the columnar zones of P1 and P2 were 0.92 ± 0.03 and 0.49 ± 0.05 (95% CL), respectively. It should be noted that the amount of austenite decreased to 0.27 ± 0.08 in the equiaxed zone of P2 as shown in Figure 7(d). Both alloys exhibited larger amounts of austenite than predicted by Software A[38] at the solidus temperature for equilibrium solidification, which suggests that solid state transformation of δ-ferrite to austenite occurred with further cooling.

Chemical analysis across the δ-ferrite and austenite interface using energy dispersive spectroscopy and spot scans every 5 to 10 μm are reported in Figures 8 and 9. Manganese and aluminum were partitioned respectively to the austenite and δ-ferrite in both alloys; however, the distribution of the elements differed in the two alloys. The manganese and aluminum were maximum within the austenite and ferrite in P1, whereas in P2 the manganese and aluminum showed maximum and minimum contents at one of the δ-ferrite and austenite interfaces, i.e. asymmetric. Chemical analyses of P2 with plate-like interfaces are reported in Figure 9 and they also show asymmetric gradients across the austenite and ferrite phases.

Electron backscattered diffraction analyses were performed and inverse pole figure maps with respect to the thermal gradient and solidification direction were used to characterize the growth of the primary δ-ferrite and the austenite in the chill, columnar, and equiaxed zones of P1 and P2 as shown in Figures 10 and 11. The chill zone was observed as being less than 50 μm from the surface. The dominant crystallographic growth direction in the chill and columnar zones for the δ-ferrite was in the <010> for both alloys. The peritectic austenite also had a preference for <110> in the columnar zone, but in general the austenite shared the same crystallographic growth direction with the δ-ferrite. In P1 59% and in P2 45% of the observations indicated that both δ-ferrite

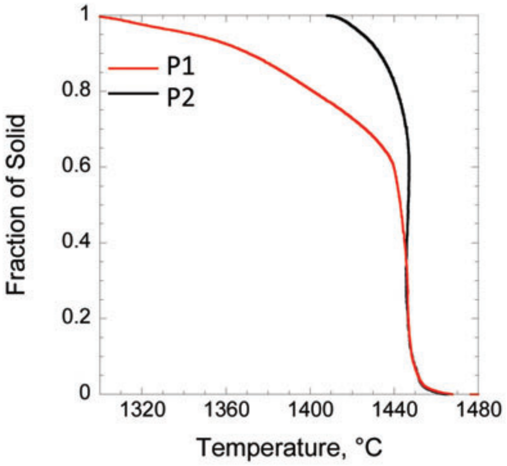

Figure 5. Cooling curves for P1 (red line) and P2 (black line). For P1, the liquidus and solidus temperatures were 1447°C (2637°F) and 1307°C (2385°F), respectively. For P2, the liquidus and solidus temperatures were 1448°C (2638°F) and 1396°C (2545°F), respectively. Alloy P2 was poured in an insulated cup and experienced a slower cooling rate than P1.

Table 4. Calculated and Measured Transformation Temperatures and Weight Fractions of δ-ferrite

		P1	P2
$T_{liquidus}$, °C	Equilibrium	1430	1435
	Scheil	1430	1435
	Measured	1447	1448
$T_{peritectic}$, °C	Equilibrium	1398	1340
	Scheil	1400	1350
$T_{solidus}$, °C	Equilibrium	1320	1312
	Scheil	1300	1245
	Measured	1307	1396
W_f of δ at $T_{peritectic}$	Equilibrium	0.37	0.87
	Scheil	0.35	0.66
	Thermal Analysis	0.37	0.65
W_f of δ at $T_{solidus}$	Equilibrium	0.16	0.84
	Scheil	0.3	0.65
W_f of δ as-solidified	Measured in Columnar (95% CL)	0.08 ± 0.03	0.51 ± 0.05

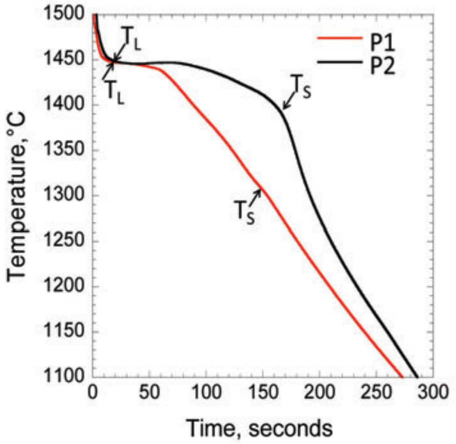

Figure 6. Fraction of solid for P1 (red line) and P2 (black line) as function of temperature depicting larger undercooling is required for the solidification of P1 after the peritectic reaction occurred.

and austenite shared the same crystallographic growth direction of either <010> or <110> in the columnar zone. As expected, the equiaxed zones for both alloys showed high deviation in the crystallographic directions relative to the thermal gradient for both δ-ferrite and austenite, which has been reported in Figures 12 and 13. Figure 14 shows the frequency of observation that an established orientation relationship existed between the δ-ferrite and austenite with less than a 10° deviation for the columnar and equiaxed zones. It should be noted that alloy P1 has a low frequency of occurrence for an orientation relationship which corroborates the observation that the peritectic austenite grows in the same crystallographic direction, <010> or <110>, as the adjacent δ-ferrite and would thus preclude the K-S orientation relationship. This result is contrary to what is often reported for similar crystallographic studies reported for the fusion zone of a tungsten inert gas (TIG) weld.

Discussion

Previous studies by Brown et al.[22] and Mataya et al.[25] reported crystallographic orientation relationships of either K-S or H-B for solidified stainless steels, but provided no quantitative information as to the frequency of occurrence. These authors[22,25] stated that their studies were not exhaustive and the region of the casting investigated was not reported. The quantitative work reported here shows that the occurrence of crystallographic orientation relationships for the peritectic austenite is dependent upon the amount of primary δ-ferrite formed. Alloys that produce more primary δ-ferrite, such as P2, are seven times more likely to exhibit a crystallographic orientation relationship for the peritectic austenite in the columnar zone. In contrast, alloys with less primary δ-ferrite, such as P1, have nearly a 60% probability of exhibiting the same crystallographic growth direction as

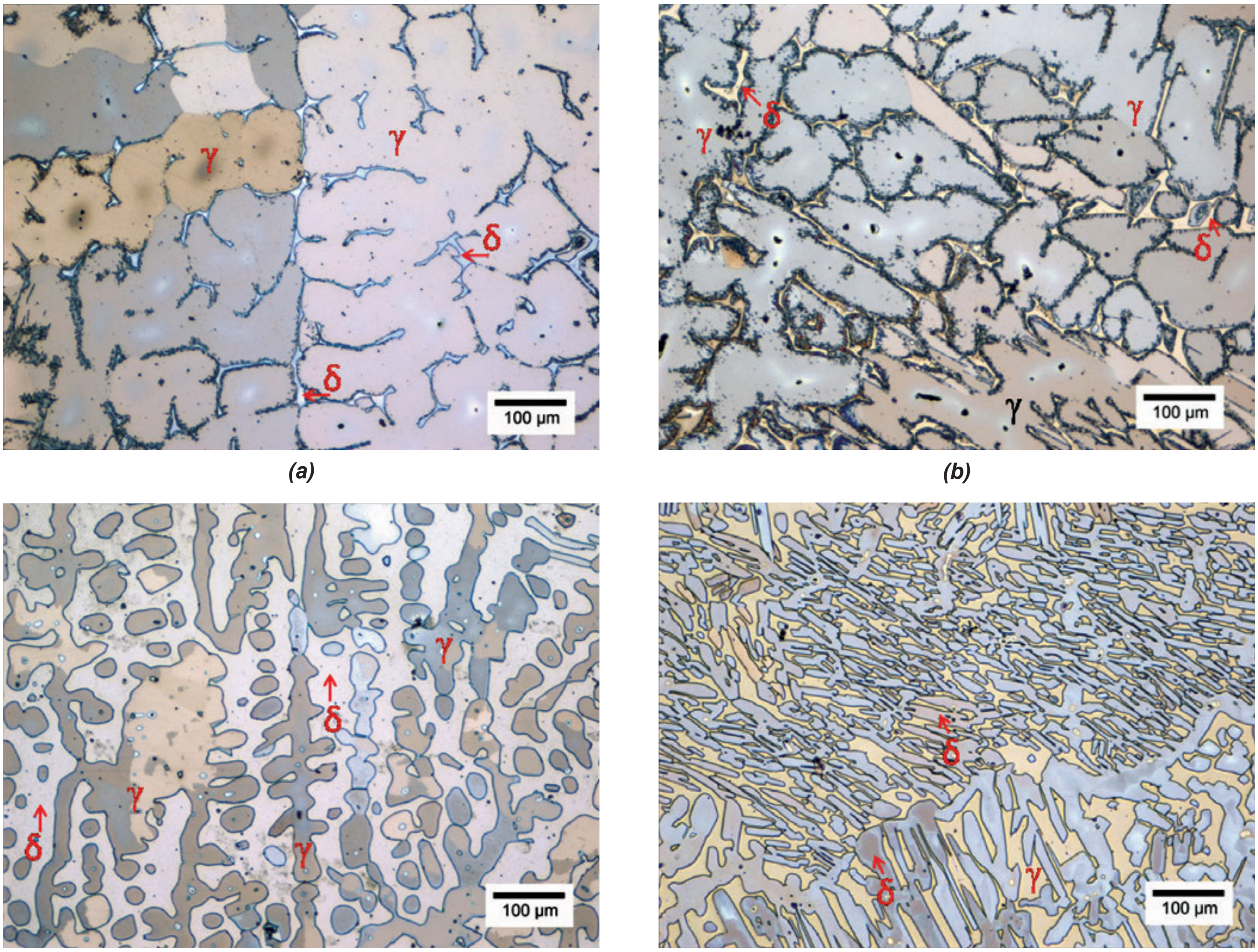

(a) (b)

(c) (d)

Figure 7. As-solidified microstructures in the (a) columnar and (b) equiaxed zones in P1 and in the (c) columnar and (d) equiaxed zones in P2. The equiaxed zone in P2 shows a predominance of the plate-like morphology with faceted interfaces. The primary δ-ferrite appears lighter than the retained austenite in all microstructures. Arrows are used to point to examples of primary δ-ferrite. Symbols (δ= ferrite and γ = austenite) were used to label phases. Alloy P1 contained secondary ferrite. The mold wall is located towards the top of each photograph. Samples were etched with 10% sodium metabisulfite.

the adjacent primary δ-ferrite and as a result only 5% of the peritectic austenite interfaces exhibit a crystallographic orientation relationship in the columnar zone. This may suggest a fundamental change in the mechanism of austenite nucleation and growth during the peritectic reaction, which is dependent upon the amount of primary δ-ferrite and perhaps the imposed thermal gradient during the peritectic reaction.

Trivedi and Somboonsuk[39] noted that the primary dendrite spacing, λ_1, is proportional to $G^{-1/2}$, where G is the thermal gradient. A comparison of the measured spacing λ_1, the frequency of observing the K-S orientation relationship and the frequency of observing the same growth direction for the peritectic austenite is shown in Table 5. A comparison of the two alloys shows that the dendrite spacing increases in proportion to the primary δ-ferrite formed. This suggests that the thermal gradient during the peritectic reaction would be lower for P2 relative to P1. Furthermore, the equiaxed zone would be expected to have a lower thermal gradient as compared to the columnar zone.[40] Here again there is a greater proportion of interfaces exhibiting an orientation relationship for the peritectic reaction in the equiaxed zone of P2. In the chill zone, rapid cooling of the peritectic austenite grains at the mold wall would be expected to occur and solidification would lead to a random orientation of austenite grains prior to the grains growing with a preferred orientation as observed in the columnar zone (Figures 12 and 13).

It is proposed here that when the amount of δ-ferrite is large, as in P2, that the thermal gradient is substantially reduced by recalesence during primary solidification. The growth of the peritectic austenite film would thus be slower and more apt to form a low surface energy interface with an orientation relationship. As a result, these low energy interfaces may

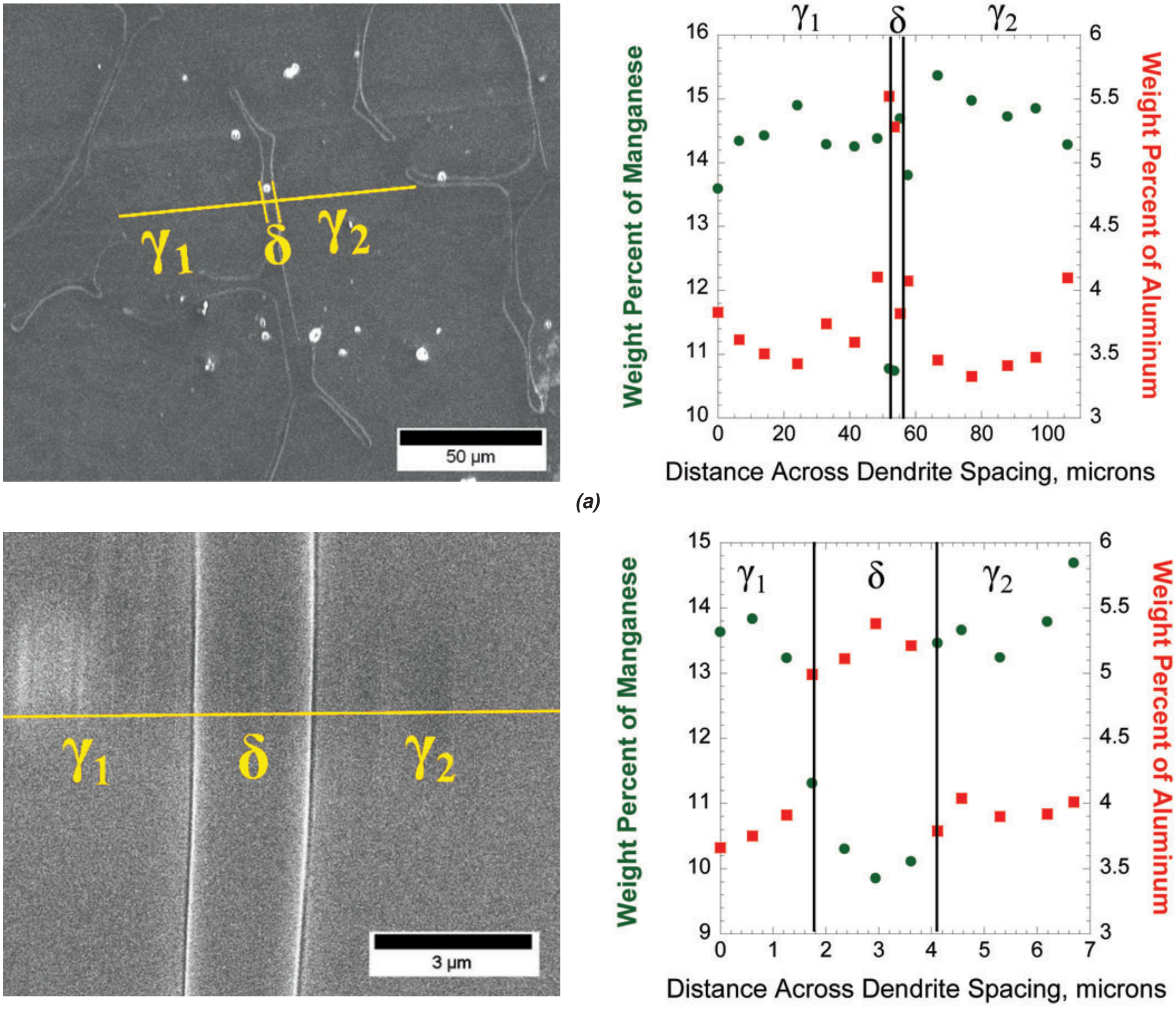

(a)

(b)

Figure 8. Secondary electron images of castings in the columnar zone of P1 showing EDS spot measurements across the δ-ferrite/austenite interface showcasing the profiles of (a) austenite and (b) skeletal δ-ferrite.

be faceted and immobile with respect to further solid state transformation to austenite. The equiaxed zone where a low thermal gradient condition was expected also produced the most faceted interfaces with a K-S orientation relationship.

In contrast, when the fraction of primary δ-ferrite is low, as in P1, the thermal gradient is sufficient to drive the growth of select austenite orientations independent of the primary δ-ferrite as observed in other systems.[9,42,43] The frequency of observing a K-S orientation relationship was reduced in P1; and thus, the interfaces were expected to be nonfaceted and more mobile; and thus, peritectic transformation (δ→γ) was more likely. The nature of the austenite nucleation and growth relative to the primary δ-ferrite would then be expected to show a different solute segregation pattern than observed in P2 where solute redistrubution was limited due to the immobility of the faceted interfaces.

The amount of δ-ferrite measured from the thermal analysis data deviated 5.7% away from the value predicted by the Scheil algorithm at the peritectic temperature in P1 while the measured amount of δ-ferrite in P2 was 1.5% greater than the Scheil prediction. In contrast, the weight fractions of δ-ferrite measured in the columnar zones of P1 and P2 were less than the calculated values at the solidus temperature which indicates a solid state peritectic transformation (δ→γ) occurred. In P1 the observed weight fraction of δ-ferrite varied 50% and 73% from the calculated equilibrium and Scheil predictions, respectively; whereas in P2 the observed weight fraction of δ-ferrite varied 39% and 22% from the calculated equilibrium and Scheil values, respectively. The discrepancies between the measured and calculated amounts of δ-ferrite are less in P2 since faceted and immobile interfaces suppressed the solid state peritectic transformation in P2 resulting in more untransformed δ-ferrite.

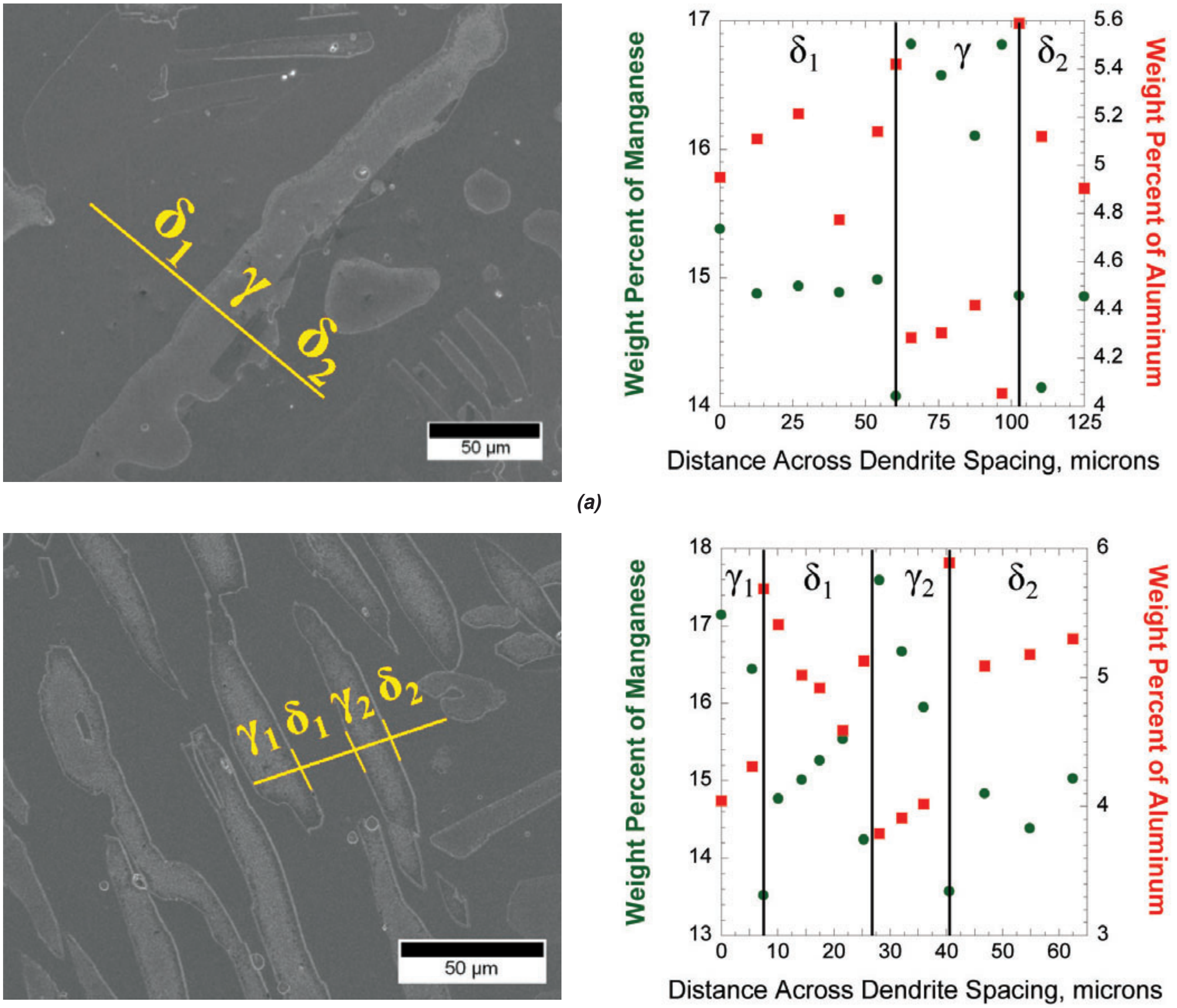

Figure 9. Secondary electron images of castings in the columnar zone of P2 showing EDS spot measurements across the δ-ferrite/austenite interface with (a) engulfing ferrite and (b) plate-like ferrite morphologies with faceted interfaces.

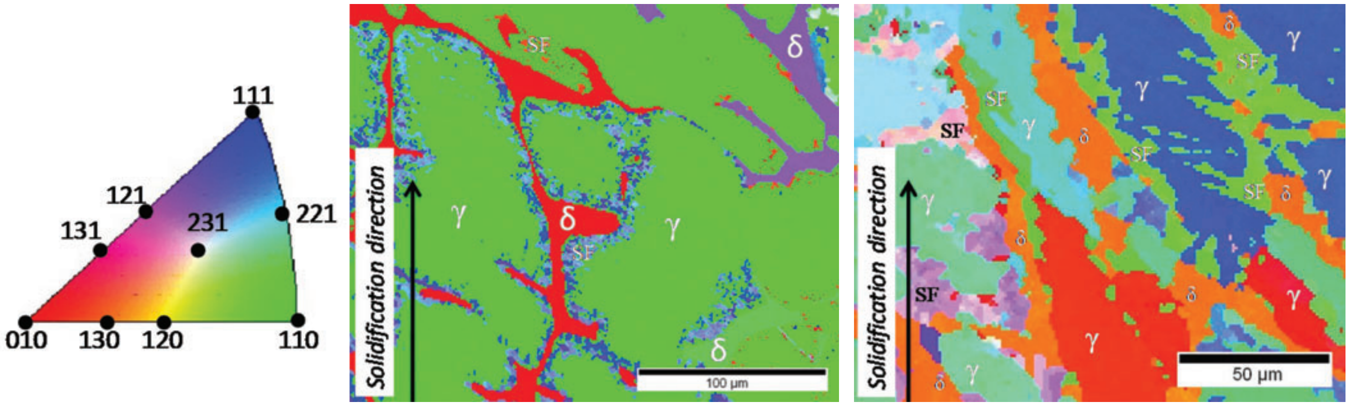

(a) Columnar Zone (b) Equiaxed Zone

Figure 10. Representative inverse pole figure mapping analysis of primary δ-ferrite (δ), secondary ferrite (SF) and austenite (γ) displayed texture in the solidification direction of the P1 casting in the (a) columnar and (b) equiaxed zones. In figure (a) the primary δ-ferrite exhibits two different orientations with respect to the austenite. The red highlighted δ-ferrite shows the expected <010> growth direction while the purple highlighted δ-ferrite has nearly a <121> which brings it close to the K-S orientation relationship with the <110> aligned austenite. Note that the secondary ferrite has two variants with one showing the near <121> orientation. The mold wall is located at the bottom of the images and was normal to the solidification direction.

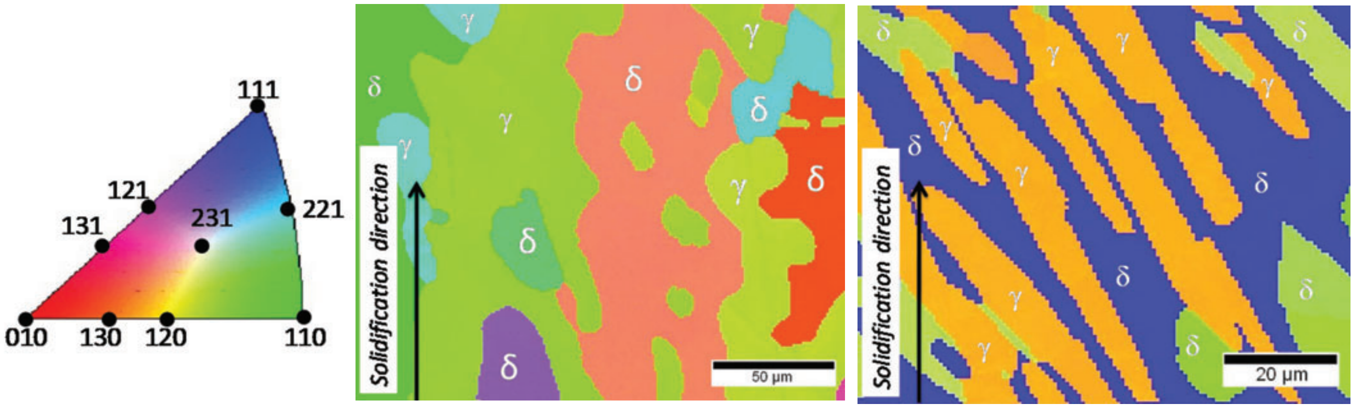

(a) Columnar Zone (b) Equiaxed Zone

Figure 11. Representative inverse pole mapping analysis of primary δ-ferrite (δ) and austenite (γ) displayed texture in the solidification direction of the P2 casting in the (a) columnar and (b) equiaxed zones. The mold wall is located at the bottom of the images and was normal to the solidification direction.

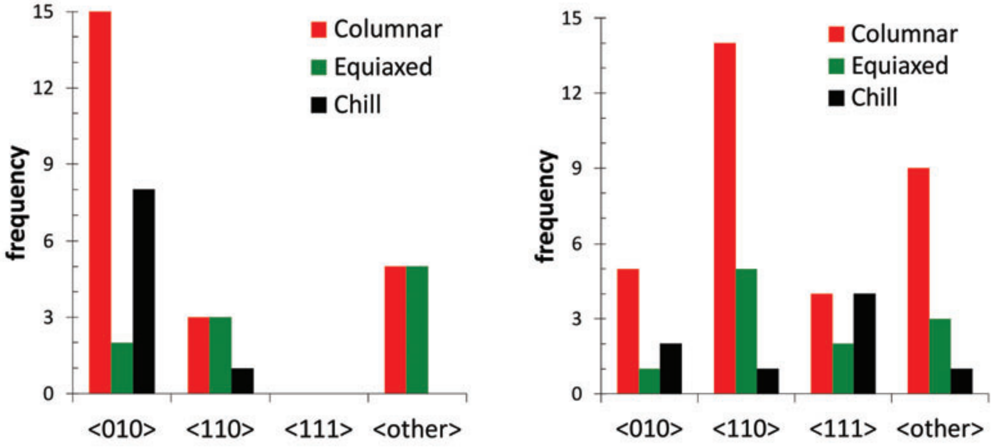

(a) Primary δ-ferrite (b) Austenite

Figure 12. Frequency of various growth directions of (a) primary δ-ferrite and (b) austenite parallel to the thermal gradient in the chill, columnar, and equiaxed zones of casting P1.

Thermodynamic predictions of liquidus, solidus, and peritectic reaction temperatures proved to be difficult using the current steel database available in Software A.[38] Measured liquidus temperatures were higher than predicted but within 13 to 17°C (23.4 to 30.6°F). Solidus temperatures were relatively close for P1, but the measured solidus temperature deviated from the calculated Scheil value towards the calculated equilibrium value. In the case of P2, the solidus temperature was 84 and 151°C (151.2 and 271.8°F) above the calculated equilibrium and Scheil solidus temperatures, respectively. These large deviations from the measured solidus temperatures indicate that the thermodynamic database for body-center cubic (bcc) and face-centered cubic (fcc) solids with aluminum contents greater than 3 wt.% may introduce greater partitioning of aluminum and manganese during solidification than actually observed.

Partition coefficients, *k*, for aluminum and manganese were calculated using Software A[38] and similar partitioning is expected in both P1 and P2 for each phase as shown in Table 6. Experimental partition coefficients were determined from the solute profiles and show relatively good agreement for P1, but significant deviation for the higher aluminum P2. Specifically, the degree of aluminum partioning is 15% less than predicted by Software A[38] and this may help explain the large deviations between measured and calculated solidus temperatures.

Based upon the calculated partition coefficients, the first δ-ferrite and first austenite to form would each be aluminum rich and manganese lean. A qualitative analysis of the vertical sections shown in Figure 3 also suggests that the first austenite to form is low in manganese while the last austenite to solidify is manganese rich. The vertical section with respect to aluminum is less informative. Austenite nucleated at the liquid/δ-ferrite interface with an orientation relationship would grow preferentially away from the interface by solidification. The solid state transformation of δ-ferrite (i.e., δ→γ peritectic trans-

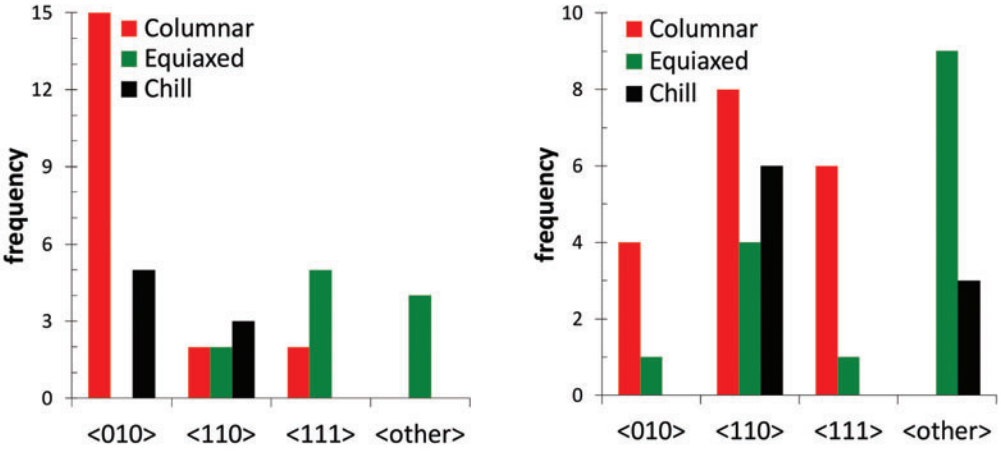

(a) Primary δ-ferrite *(b) Austenite*

Figure 13. Frequency of various growth directions of (a) primary δ-ferrite and (b) austenite parallel to the thermal gradient in the chill, columnar, and equiaxed zones of casting P2.

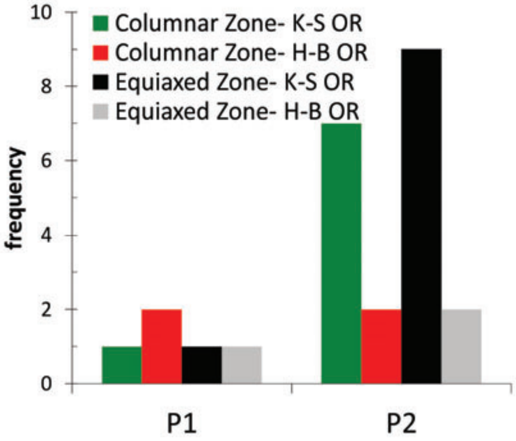

Figure 14. Frequency that K-S or H-B orientation relationship (OR) was observed in the columnar and equiaxed zones of P1 and P2 castings.

Table 5. Comparison of Primary Dendrite Spacing, λ_1

Location	λ_1, μm (95% CL)	Frequency of K-S orientation relationship	Frequency of same <hkl> of adjacent δ and γ
P1 (0.35δ)			
Columnar	43.2 ± 11.9	0.05	0.59
Equiaxed	*	0.10	0.30
P2 (0.66δ)			
Columnar	93.4 ± 16.7	0.35	0.45
Equiaxed	*	0.65	0.15

* λ_1 not reported since castings do not have well-defined dendrite spacing in the equiaxed zone as stated in the ASM handbook.[41]

formation) would be slow because the faceted interface structure would be coherent or semi-coherent and inherently less mobile than an incoherent interface. Comparisons of the austenite weight fractions in the columnar and equiaxed zones as well as the solute profiles across faceted and nonfaceted microstructures confirm this hypothesis. A comparison of the columnar and equiaxed zones of P2 show that the amount of austenite is greater (0.49 vs. 0.27 in Figure 7) in the columnar zone and less likely (0.35 vs. 0.65 in Table 5) to show a faceted interface resulting from an orientation relationship. Figure 15 illustrates the asymmetric solute profile across the peritectic interface reflecting the solute profile expected for a faceted or immobile interface with an orientation relationship. Specifically, the manganese concentration along one of the δ-ferrite interfaces should be a minimum and the manganese concentration increases with distance from the peritectic reaction ($L+\delta \rightarrow \gamma$) interface into the austenite. In a similar fashion, the first austenite along the δ-ferrite interface should be higher in aluminum content and decrease as the austenite grows. This profile was observed for P2 across a faceted interface (Figure 9b). Brooks et al.[11] showed more symmetric profiles where the cores of the austenite and vermicular ferrite showed maximums and minimums in the profiles. They reasoned this was due to solute partitioning during solid state transformations upon cooling, which would suggest a mobile interface existed. The study of Brooks et al.[11] did not include the crystallographic orientation of the ferrite or austenite. A similar concentration profile with local minimums and maximums in solute concentrations within the respective phases was observed in P1 as shown in Figure 8. Using the experimentally determined compositions of the δ-ferrite and austenite at the peritectic interface as two input streams in Software A[38] resulted in an increase in austenite at the peritectic temperature. This would indicate that solid state transformation would be favorable when the interface was mobile, i.e. a nonfaceted interface. Evidence for this reaction may be gleaned from the microstructures shown for P1 (Figure 7). The shape of the interface between the austenite and the δ-ferrite suggest diffusional growth of austenite into the δ-ferrite. The resultant austenite composition would then be higher in aluminum and lower in manganese; and thus, more apt to transform to α-ferrite upon cooling as observed in the microstructure.

Studies performed by Fredriksson et al.[20] on peritectic solidification in binary alloys showed that the mode of the peritectic solid product nucleated and grew dependant on the weight fraction of primary solid. When the primary phase had a weight fraction greater than 0.45 the peritectic solid product grew in contact with the primary phase in their study.[20] Conversely, the Al-11Mn alloy showed that the peritectic solid product precipitated without contact

Table 6. Comparison of Calculated and Experimental Partition Coefficients, k

	Software A[38] - P1			Experimental -P1	Software A[38] - P2			Experimental –P2
Solute	$k^{\delta/l}$	$k^{\gamma/l}$	$k^{\delta/\gamma}$	$k^{\delta/\gamma}$	$k^{\delta/l}$	$k^{\gamma/l}$	$k^{\delta/\gamma}$	$k^{\delta/\gamma}$
Mn	0.62	0.82	0.76	0.70	0.64	0.83	0.77	0.80
Al	1.90	1.25	1.52	1.47	1.59	1.09	1.46	1.24

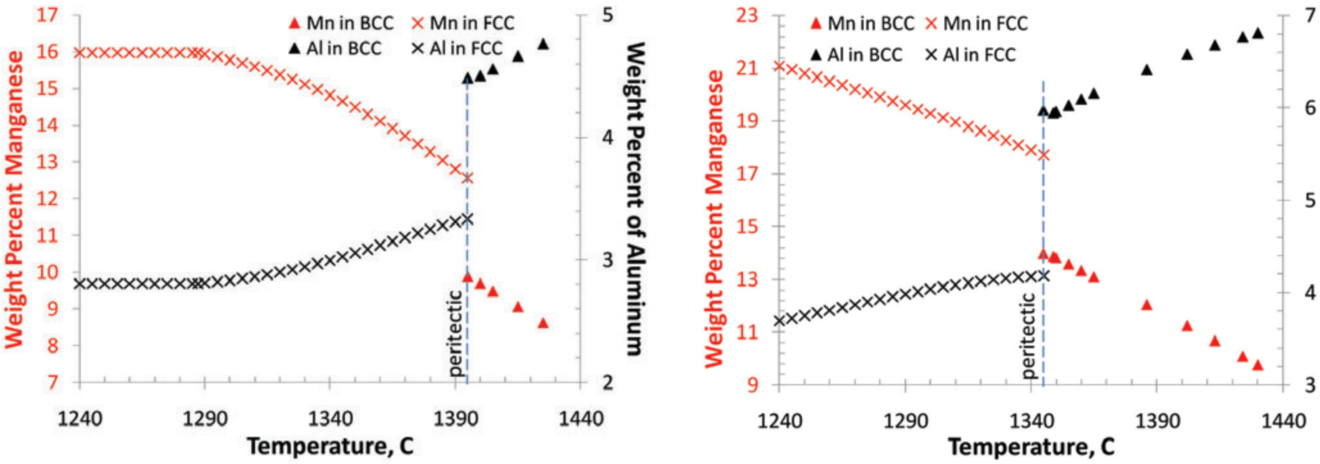

(a) *(b)*

Figure 15. Aluminum and manganese predicted composition profiles for the interface at the peritectic reaction for (a) P1 and (b) P2. Compositions at temperatures above and below the peritectic tempertaure represent the δ-ferrite and austenite, respectively, profiles. The line at the peritectic temperatures shows the composition of the ferrite and austenite interface.

when the primary solid phase was 0.25.[20] Results reported here for both P1 and P2 show the austenite forms a film at the δ-ferrite/liquid interface during the peritectic reaction regardless of the weight fraction of primary δ-ferrite formed when in the range of 0.35 to 0.66. This was determined based on the concentration profiles observed where the interfaces consistently agreed with the expected chemistry of the first austenite to form as being high in aluminum and low in manganese.

The amount of primary δ-ferrite can affect the crystallography of the peritectic austenite. Large fractions of primary δ-ferrite decrease the thermal gradient and promote interfaces that are faceted and have either the K-S or the H-B orientation relationship. At low weight fractions of primary δ-ferrite, a high thermal gradient favors a peritectic austenite with a faster growth direction, i.e. <100> and <110> in the columnar zones. The resultant microstructures are less likely to exhibit an orientation relationship.

The dendrite coherency point (DCP) temperature was derived from the thermal analysis data to study the effects of the weight fraction of primary δ-ferrite on casting properties in duplex steels. The DCP is defined as the transition stage during solidification from mass feeding to interdendritic feeding where an impinging dendrite network has formed. The interlocking of the dendrites would affect fluidity of the alloy and thus affect casting defects such as porosity, macrosegregation, and hot tearing, which occur after the DCP. The DCP temperature can be identified as an extreme in the second derivative curve of temperature with respect to time.[44] An example for determining the fraction of solid at the DCP and the temperature is shown in Figure 16 for P1. A minimum of the second derivative of temperature was used to estimate the fraction of solid (see Figure 16a). The fraction of the solid was then used to identify the DCP temperature (see Figure 16b). The fractions of solid at the DCP were 0.4 and 0.34 for P1 and P2, respectively. The DCP temperature was between 1445 and 1446°C (2601 and 2603°F) for both alloys. The fluidity of P1 would be expected to be greater than P2, since the DCP of P1 occurred at a higher solid fraction.

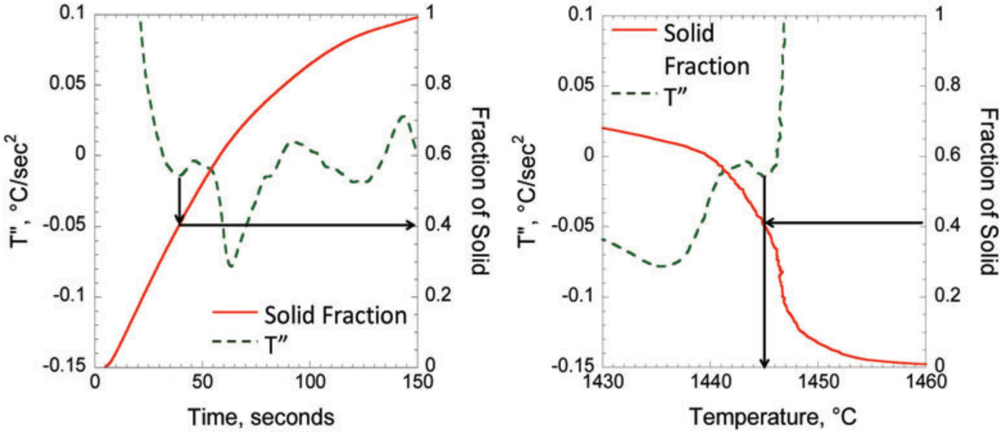

(a) (b)

Figure 16. Fraction of solid as a function of (a) time and (b) temperature for P1. The dendrite coherency point was determined by the minimum of the second derivative shown in (a) and then used to determine the dendrite coherency temperature in (b).

St John et al.[45] described the cooling curve for peritectic solidification as possessing a thermal arrest during the peritectic reaction of L+δ→γ. As the reaction proceeds, the austenite encapsulates the δ-ferrite and thus the rate for solidification decreases and a larger undercooling is required for austenite formation. The solidification rate is then controlled by the peritectic transformation. A similar observation has been reported by Dash et al.[46] for Cr and Mo steels, i.e. SAE grade 4122. Additions of nickel greater than 3 wt.% to the Cr and Mo steel suppressed the peritectic reaction and the melt solidified directly to austenite. There was no change in the slope of solidification with respect to temperature for the high nickel alloys until the fraction of solid was approximately 0.9.[46] The results reported in this study show the change in slope occurred at a lower fraction of solid (0.37) when less δ-ferrite formed (i.e. P1) whereas when a greater fraction of δ-ferrite formed (i.e. P2) the slope decreased when the fraction of solid was 0.65. Both solid values are relatively close to the amount of primary δ-ferrite predicted by Software A[38] using the Scheil model.

Cast stainless steels often show duplex microstructures of δ-ferrite and austenite. CF8 is a common austenitic grade that produces a vermicular ferritic structure similar to P1.[47] Based upon the crystallographic analysis reported here, these alloys would be susceptible to early fatigue crack nucleation since the majority of the interfaces would not exhibit the K-S orientation relationship.[3] In contrast, the duplex stainless steels such as 25-07 would exhibit the engulfing ferrite microstructure and faceted interfaces with the K-S orientation relationship.[2,48] These interfaces would be more resistant to interphase crack nucleation.[3] In contrast to crack nucleation, crack propagation with respect to the interphase crystallography behaves in the opposite fashion. Interfaces having the K-S orientation relationship allow easy crack propagation through the interface whereas crack deflection at the interface occurs in the absence of the orientation relationship.[2] The importance of fatigue crack nucleation versus propagation is dependent upon low cycle versus high cycle design expectations.[49] In low cycle fatigue, crack propagation represents a greater portion of the fatigue life.

Conclusion

High aluminum and manganese sand cast alloys studied here showed that peritectic austenite has a preference of <110> growth that increases in concentration from the chill zone to the columnar zone. This observation suggests that the growth of the peritectic austenite film can be competitive with austenite films aligned for <110> growth being favored. The crystallography of the peritectic austenite with respect to δ-ferrite was found to depend upon the amount of primary δ-ferrite formed during solidification. At low weight fractions of primary δ-ferrite (0.35 in P1), the peritectic austenite adopts a fast growth direction rather than form an orientation relationship with the primary δ-ferrite. The peritectic austenite was more likely to form a K-S or a H-B orientation relationship as the amount of primary δ-ferrite increased or the thermal gradient decreased. In P2 (δ-ferrite weight fraction of 0.66) the peritectic austenite was 7 times more likely than P1 to have the K-S orientation relationship in the columnar zone and the frequency of occurrence for an orientation relationship doubled in the equiaxed zone.

Solute profiles were used to show that the mechanism of the peritectic reaction in a casting is independent of the amount of primary δ-ferrite formed and proceeds by the formation of a continuous austenite film along the δ-ferrite. The interface structure, however affects the peritectic transformation (solid state δ→γ). Faceted interfaces associated with an orientation relationship are less mobile and inhibit the solid state peritectic transformation. The equiaxed zone of casting P2, which contained the highest percentage of interfaces with the K-S orientation relationship, exhibited nearly the same amount of δ-ferrite as expected at the solidus temperature indicating a significant suppression of the peritectic transformation.

A higher fraction of solids formed in P1 prior to the dendrite coherency point, which suggests better fluidity and castability when the amount of primary δ-ferrite is less. Good agreement between the thermal analysis and the calculated fraction solid prior to the peritectic reaction was obtained for the high manganese and aluminum alloys; however, the calculated partition coefficients at the higher aluminum content of 5.58% varied from the experimentally determined values suggesting that the thermodynamic models for high aluminum steels are in need of further work.

The results reported here may also shed some insight with regard to developing dual phase alloys with improved fatigue crack propagation resistance. A low weight fraction of primary δ-ferrite or a high thermal gradient would be required in cast alloys to improve low cycle fatigue performance by suppressing the formation of the K-S orientation relationship.

Acknowledgements

This work was supported in part by the National Science Foundation (NSF) and the Department of Energy under contract CMMI 0726888. The FEI Helios NanoLab dual beam FIB was obtained with a Major Research Instrumentation grant from NSF under contract DMR-0723128. The authors gratefully acknowledge the support of the Graduate Center for Materials Research and in particular Dr. Ming Zhang for help with the EBSD study. Dr. S. Lekakh is gratefully acknowledged for helpful discussions on thermal analysis. Meghan McGrath was supported by a Department of Education GAANN fellowship under contract P200A0900048.

REFERENCES

1. Kim, S., Marrow, T.J., “Application of Electron Backscattered Diffraction to Cleavage Fraction in Duplex Stainless Steel,” *Scripta Materialia*, vol. 40 no. 12, pp. 1395 (1999).
2. Marinelli, M.C., Bartali, A.E., Signorelli, J.W., Evrard, P., Aubin, V., Alvarez-Armas, I., Degallaiz-Moreuil, S.,“Activated Slip Systems and Microcrack Path in LCF of a Duplex Stainless Steel,” *Materials Sci. and Eng. A*, vol. 509, pp. 81-88 (2009).
3. Bugat, S., Besson, J., Gourgues, A.-F., N’Guyen, F., Pineau, A., “Microstructure and Damage Initiation in Duplex Stainless Steels,” *Materials Sci. and Eng. A*, vol. 317, pp. 32-36 (2001).
4. Suutala, N., Takalo, T., Moisio, T., “Single-Phase Ferritic Solidification Mode in Austenitic-Ferritic Stainless Steel Welds,” *Met Trans*., vol. 10A, pp. 1183-1190 (1979).
5. Inoue, H., Koseki, T., Ohkita, S., Fuji, M., “Formation Mechanism of Vermicular and Lacy Ferrite in Austenitic Stainless Steel Weld Metals,” *Science and Technology of Welding and Joining,* vol. 5, no. 6, pp. 385-396 (2000).
6. Iamboliev, T., Katayama, S., Matsunawa, A., “Interpretation of Phase Formation in Austenitic Stainless Steel Welds,” *Welding Research Journal*, pp. 337-347 (Dec 2003).
7. Huang, Y.M., Wu, Y.M., Pan, C.X., “EBSD Study of Solidification Characteristics of Austenitic Stainless Steel Weld Pool,” *Materials Science and Technology*, vol. 26, no 6, pp. 750-753 (2010).
8. Stefanescu, D.M. *Science and Engineering of Casting Solidification,* 2nd edition, Springer (2009).
9. Kerr, H.W., Cisse, J., Bolling, G.F.,“On Equilibrium and Non-Equilibrium Peritectic Transformations,” *Acta Met*., vol. 22, pp. 677-684 (1974).
10. Chalmers, B., *Physical Metallurgy*, John Wiley & Sons, New York (1964).
11. Brooks, J.A., Williams, J.C., Thompson, A.W., “Microstructural Origin of the Skeletal Ferrite

Morphology of Austenitic Stainless Steel Welds," *Met Trans. A,* vol. 14, pp. 1271-1281 (1983).

12. Ueshima, Y., Mizoguchi, S., Matsumiya, T., Kajioka, H., "Analysis of Solute Distribution in Dendrites of Carbon Steel with δ/γ Transformation during Solidifications," *Met Trans. B*, vol. 17, pp. 845-859 (1986).
13. Aritomi, N., Dan, T., Kimura T., Ogawa, K., "Microsegregation of Aluminum, Silicon and Manganese in Fe-10mass%Ni Alloy Ingot," *Materials Sci. and Eng. A,* vol. 102, pp. 85-95 (1988).
14. Shibata, H., Arai, Y., Suzuki, M., Emi, T., "Kinetics of Peritectic Reaction and Transformation in Fe-C Alloys," *Met Trans. B*, vol. 31, pp. 981-991 (2000).
15. Dhindaw, B.K., Antonsson, T., Tinoco, J., Fredriksson, H., "Characterization of the Peritectic Reaction in Medium-Alloy Steel through Microsegregation and Heat-to-Transformation Studies," *Met Trans. A*, vol. 35, pp. 2869-2879 (2004).
16. Bosze, W.P. and Trivedi, R., "On the Kinetic Expression for the Growth of Precipitate Plates," *Met. Trans. A*, vol. 4, pp. 511-512 (1974).
17. "Peritectic Solidification," *ASM Handbook*, *Vol. 15 Casting* edited by D.M. Stefanescu, ASM International, pp. 330-337 (2008).
18. Hu, H., "On Kurdjumov-Sachs Orientation Relationship in Successive Phase Transformations," *Transactions of the Metallurgical Society of AIME,* vol. 233, pp. 1071-1075 (1965).
19. Inoue, H., Koseki, T., Okita, S., Fuji, M., "Solidification and Transformation Behavior of Austenitic Stainless Steel Weld Metals Solidified as Primary Ferrite: Study of Solidification and Subsequent Transformation of Cr-Ni Stainless Steel Weld Metals (2nd report)" *Welding International,* vol. 11, no 12, pp. 937-949 (1997).
20. Fredriksson, H., Nylén, T.,"Mechanism of Peritectic Reactions and Transformations," *Materials Sci. and Tech.*, vol. 16, pp. 283-294 (1982).
21. Suutala, N., Takalo, T., Moisio, T., "Ferritic-Austenitic Solidification Mode in Austenitic Stainless Steel Welds," *Met. Trans. A*, vol. 11, pp. 717-725 (1980).
22. Brown, E.L., Whipple, T.A., Krauss, G., "Metallography of Duplex Stainless Steel Castings," *Duplex Stainless Steels,* ASM, pp. 665-691(1980).
23. Fukumoto, S. and. Kurz, W., "The δ to γ Transition in Fe-Cr-Ni Alloys during Laser Treatment", *ISIJ International*, vol. 37, no. 7, pp. 677-684 (1997).
24. Headley, T.J., Brooks, J.A., "A New BCC-FCC Orientation Relationship Observed between Ferrite and Austenite in Solidification Structures of Steels," *Met Trans. A,* vol. 33, pp. 5-15 (2002).
25. Mataya, M.C., Nilsson, E.R., Brown, E.L., Krauss, G., "Hot Working and Recrystallization of As-Cast 316L," *Met Trans. A*, vol. 34, pp. 1683-1703 (2003).
26. Inoue, H., Koseki, T., "Proposal of Independent Two Phase Growth during Solidification in Austenitic Stainless Steels," *Proceedings of the 7th International Conference on Trends in Welding Research,* Pine Mountain, GA, pp. 29-34 (May 2005).
27. Elmer, J.W., Allen, S.M., Eagar, T.W., "Microstructural Development during Solidification of Stainless Steel Alloys," *Met Trans. A*, vol. 20, pp. 2117-2131 (1989).
28. Elmer, J.W., "The Influence of Cooling Rate on the Microstructure of Stainless Steel Alloys," PhD thesis, Lawrence Livermore National Laboratory (1988).
29. Brooks, J.A., Williams, J.C., Thompson, A.W., "STEM Analysis of Primary Austenite Solidified Stainless Steel Welds," *Met Trans. A*, vol. 14, pp. 23-31 (1983).
30. Kurdjumov, G., Sachs, G., *Z Phys.*, vol. 64, pp. 325-43 (1930).
31. Porter, D.A., Easterling, K.E., Sherif, M.Y., *Phase Transformations in Metals and Alloys*, 2nd ed., CRC Press (2009).
32. McGrath, M., Van Aken, D.C., Richards, V., "Mechanical Properties and Their Dependence on Microstructures in Hot-Rolled 3rd Generation Advanced High Strength Steel," *TMS 2010 Proceedings*, Seattle, OR (February 2010).
33. Van Aken, D.C., Medvedeva, J.E. , McGrath, M.C. , Medvedeva, N.I., Richards, V.L., "Developing Lightweight Steels for the Transportation Industry," *Proceedings of 2009 NSF Engineering Research and Innovation Conference,* Materials Processing and Manufacturing (MPM), Honolulu, Hawaii (June 2009).
34. Van Aken, D.C., Medvedeva, J.E., McGrath, M.C., Medvedeva, N.I., Richards, V.L., "Developing Lightweight Steels for the Transportation Industry," *Proceedings of 2011 NSF Engineering Research and Innovation Conference*, Materials Processing and Manufacturing (MPM), Atlanta Georgia (2011).
35. McGrath, M., D.C. Van Aken, J. Medvedeva, V. Richards, and N. Medvedeva, "Mechanical Properties Dependence on Microstructures of Hot Rolled 3rd Generation Advanced High Strength Steels," *Steel Product Metallurgy and Applications, MS&T 2010 Conference Proceedings,* Houston, TX, pp. 1926-1940 (Oct 2010).
36. Lekakh, S.N., Richards, V.L., "Determining Solidification Parameters of Alloy Steels," *AFS Trans.,* vol. 119, pp. 521-528 (2011).
37. Djurdjevic, M.B., Kierkus, W.T., Byczynski, G.E. , Stockwell, T.J., Sokolowski, J.H. "Modeling of Fraction Solid for 319 Aluminum Alloy," *AFS Trans.,* vol. 107, pp. 173-179 (1999).
38. Thermfact and FTT-Technologies, FactSage 6.2, Aachen, Germany (2009).
39. Trivedi, R. and Somboonsuk, K. "Constrained Dendritic Growth and Spacing," *Materials Science and Engineering,* vol. 65, pp. 65-74 (1984).
40. Kurz, W. and Fisher, D.J., *Fundamentals of Solidifications*, Trans Tech Publications, Switzerland (1989).

41. Gokhale, A.M., *Metallography and Microstructures, Vol. 9*, *ASM Handbook*, ASM International, pp. 428-447 (2004).
42. Titchener, A.P., Spittle, J.A.,"The Microstructures of Directionally Solidified Alloys that Undergo a Peritectic Transformation," *Acta Met.*, vol. 23, pp. 497-502 (1975).
43. Babu, S.S., Elmer, J.W., David, S.A., Quintana, M.A., "In Situ Observations of Non-equilibrium Austenite Formation During Weld Solidification of an Fe-C-Al-Mn Low-Alloy Steel," *Proc. R. Soc. Lond. A*, vol. 458, pp. 811-821 (2002).
44. Jiang, H., Kierkus, W.T., Sokolowski, J.H., "Determining Dendrite Coherency Point Characteristics of Al Alloys Using Single-Thermocouple Technique," *AFS Trans.,* vol. 107, p. 169 (1999).
45. StJohn, D.H., "The Peritectic Reaction," *Acta Met.*, vol. 38, no. 4, pp. 631-636 (1990).
46. Dash, A., Lekakh, S. N., Richards, V.L., Van Aken, D.C., "Effect of Ni on Fluidity of Cr-Mo Steels," *AFS Proceedings of the 116th Metalcasting Congress,* Paper 12-030, Columbus, OH (April 17-21, 2012).
47. James, L.A., Mills, W.J. "Fatigue-Crack Propagation and Fracture Toughness Behavior of Cast Stainless Steels," *Engineering Fracture Mechanics*, vol. 29, no. 4, pp. 423-434 (1988).
48. Marinelli, M.C., Alvarez-Armas, I., Degallaiz, S., 10th International Conference on the Mechanical Behavior of Materials, ICM10, Busan, Korea, (May 2007).
49. Alvarez-Armas, I., Knobbe, H., Marinelli, M.C., Balbi, M., Herenu, S., Krupp, U., "Experimental Characterization of Short Fatigue Crack Kinetics in an Austeno-Ferritic Duplex Steel," *Procedia Eng.,* vol. 10, pp. 1491-1496 (2011).